ZrN-Based Flexible Resistive Switching Memory

Dayanand Kumar, Umesh Chand, Lew Wen Siang, and Tseung-Yuen Tseng, *Fellow, IEEE*

***Abstract*— In this letter, ZrN-based resistive random access memory (RRAM) is investigated for flexible memory applications for the near future. Due to the room-temperature fabrication process, the device is suitable for low-temperature flexible monolithic technologies. The TiN/ZrN/TiN device exhibits excellent AC endurance cycling (10^7), a rapid speed (45 ns) and stable retention (10^4 s) at 100°C without any degradation. In addition, RRAM devices built with an additional HfN interface layer exhibit small operational voltage variations and stable switching characteristics. The flexibility of the device is excellent, and it maintains excellent electrical characteristics at a bending radius of up to 4 mm.**

***Index Terms*— RRAM, nitrogen ions, conductive filament, resistive switching.**

I. Introduction

RESISTIVE random access memory (RRAM) has received a substantial amount of attention for use in high-density memory applications [1], [2]. Flexible electronics are becoming an evolving technology due to their attractive properties and high degree of flexibility for portable electronic devices that can be used in daily life. Flexible electronic devices are fabricated on plastic substrates and not Si substrates, so they are low-cost and green electronic devices [3]. It is well known that high local temperature and self-heating effects in the filament region can result in uncontrolled filament issues, such as switching current overshoot and reliability problems [4]. Various transition metal nitrides, such as HfN, ZrN, VN, SiN, SiCN, and CrN, have been used as either resistive switching (RS) layers or interface layers in RRAM devices [2], [5]–[8]. Transition metal nitride ZrN has a high thermal conductivity (50 W/mK) and a semiconducting phase [8]. These properties are beneficial for suppressing local heating effects and improving the controllability of the conductive filament. Several types of flexible RRAM have been reported but are not appealing due to their poor endurance, high bending radius, low speeds and poor bending cycling behavior [9]–[17]. Kim and Choi [9] reported flexible RRAM, which showed good retention (10^4 s) but poor endurance (150 cycles) and a high bending radius (10 mm). Qian *et al.* [10] also reported flexible devices with poor endurance (800 cycles), poor retention (10^3 s), a high bending radius (14 mm), and poor bending cycling behavior (850 cycles). To overcome these problems in flexible devices, we propose a flexible RRAM based on a new TiN/HfN/ZrN/TiN structure that has shown excellent characteristics, such as AC endurance (10^7 cycles), speed (45 ns), bending radius (4 mm) and retention (10^4 s) at 100°C. These characteristics indicate that the TiN/HfN/ZrN/TiN RRAM stack is better than the previously reported RRAM stacks for flexible nonvolatile memory applications. Table I shows a comparison of oxide- and organic material-based flexible devices with the current work.

TABLE I
COMPARISON OF PREVIOUS REPORTED OXIDES AND ORGANIC MATERIALS BASED FLEXIBLE DEVICES WITH CURRENT WORK

Device Structure	Endurance (Cycles)	Speed	Retention	Bending radius (mm)	Bending cycles	Report Year
Ni/Sm_2O_3/ITO/PET	10^3	------	10^5 s @ 85°C	5	10^3	2013
Cu/WO_3/ITO	10^3	------	10^5 s @ 85°C	5.5	10^3	2016
Ag/TiO_2/ITO/PET	10^2	------	------	5	500	2016
ZnS/Ti/Al_2O_3/MgO/ZnS	150	------	10^4 s	10	10^2	2017
Pt/TiO_2/ITO/PET	600	------	10^4 s	20	10^3	2017
ITO/hBN/FLG/PET	800	------	10^3 s	14	850	2017
Ni/NbO_2/Ni	420	------	10^4 s @ 85°C	5	10^3	2018
Al/P4/ITO/PET	500	10 ms	10^4 s	5	10^2	2019
Al/parylene/W	500	10 µs	10^5 s	10	500	2016
TiN/HfN/ZrN/TiN	10^7	45 ns	10^4 s @ 100°C	4 mm	10^4	This work

In this work, we demonstrate a new TiN/ZrN/TiN device on a polyethylene terephthalate (PET) substrate for emerging nonvolatile RRAM for flexible applications. The highly flexible TiN/ZrN/TiN device shows excellent switching characteristics with an on/off resistance ratio ($>10^2$), device speed (45 ns), AC endurance (10^7 cycles) and stable retention (10^4 s) at 100°C. The RS mechanism of the device is based on the formation and rupture of conductive filaments (CFs) in the ZrN layer due to nitrogen vacancies. In addition, we used HfN as a thin layer that is inserted between the top electrode and ZrN layer to reduce the voltage variation in the device.

II. Device Fabrication

First, the TiN bottom electrode (BE) was deposited by sputtering on a flexible PET substrate. A 10 nm-thick ZrN RS layer was deposited on the TiN BE by rf sputtering. Finally, a 100 nm TiN top electrode (TE) with a diameter of 100 μm using a metal shadow mask was deposited by sputtering at room temperature to form a TiN/ZrN/TiN device. In addition, 3 nm HfN was used as an interface layer between the

Manuscript received February 11, 2020; revised February 24, 2020 and March 12, 2020; accepted March 13, 2020. Date of publication March 17, 2020; date of current version April 24, 2020. This work was supported by Ministry of Science and Technology, Taiwan, under Project NSC 105-2221-E-009-134-MY3. The review of this letter was arranged by Editor B. Govoreanu. *(Corresponding author: Tseung-Yuen Tseng.)*

Dayanand Kumar is with the Institute of Electronics, National Chiao Tung University, Hsinchu 30010, Taiwan, and also with the School of Electrical and Electronic Engineering, Nanyang Technological University, Singapore 637371.

Umesh Chand is with the Department of Electrical and Computer Engineering, National University of Singapore, Singapore 117576.

Lew Wen Siang is with the School of Physical and Mathematical Sciences, Nanyang Technological University, Singapore 637371.

Tseung-Yuen Tseng is with the Institute of Electronics, National Chiao Tung University, Hsinchu 30010, Taiwan (e-mail : tseng@cc.nctu.edu.tw).

Color versions of one or more of the figures in this letter are available online at http://ieeexplore.ieee.org.

Digital Object Identifier 10.1109/LED.2020.2981529

0741-3106 © 2020 IEEE. Personal use is permitted, but republication/redistribution requires IEEE permission.
See https://www.ieee.org/publications/rights/index.html for more information.

Authorized licensed use limited to: Nanyang Technological University. Downloaded on May 09,2020 at 07:26:29 UTC from IEEE Xplore. Restrictions apply.

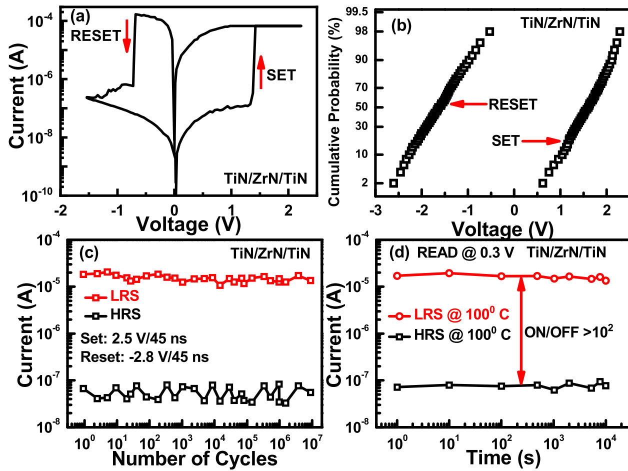

Fig. 1. (a) I-V trend for TiN/ZrN/TiN device, (b) voltage distribution of the device, (c) AC endurance of the device and (d) retention results at 100°C.

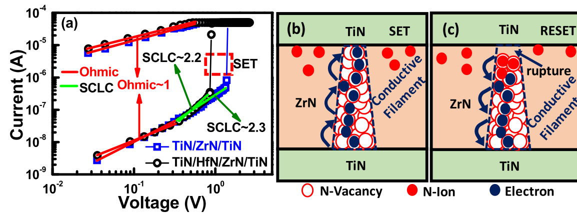

Fig. 2. (a) (color online) Replot of the I-V curve fitting for the TiN/ZrN/TiN and TiN/HfN/ZrN/TiN in both the LRS and HRS. (b) and (c) illustrate the conductive filament model for the SET and RESET of the TiN/ZrN/TiN device.

TiN and ZrN for comparison to suppress the operational voltage variation. An Agilent B1500A semiconductor parameter analyzer was used for the DC measurements, and an AC pulse was generated by an Agilent B1530A waveform generator/fast measurement unit (WGFMU). The TiN BE was grounded, and the voltage was applied to the TiN TE for the device measurements.

III. Results and Discussion

Fig. 1(a) shows the bipolar RS behavior of the TiN/ZrN/TiN device with a SET voltage (∼1.3 V) and a RESET voltage (∼ −0.8 V). Figure 1(b) depicts the voltage distribution of the device during 100 continuous DC switching cycles. The device exhibits a wide variation in the SET/RESET voltages during the continuous switching cycles. Such a wide variation is due to the random formation and rupture of the CF in the TiN/ZrN/TiN device. The reliability test is also characterized to confirm the memory performance of the device, as shown in Fig. 1(c). The AC endurance of the device was determined by using a pulse height of 2.5 V for the SET operation and −2.8 V for the RESET operation under a pulse width of 45 ns at a read voltage of 0.3 V. A large AC endurance of more than 10^7 switching cycles is achieved. The retention characteristics are also measured for the device, which is shown in Fig. 1(d). Both the low resistance state (LRS) and high resistance state (HRS) are highly stable for more than 10^4 s without any degradation at 100°C.

To study the conduction mechanisms of TiN/ZrN/TiN and TiN/HfN/ZrN/TiN devices, the I–V curves of the devices in the positive voltage region were redrawn using a log-log scale, as shown in Fig. 2(a). According to the space-charge limited conduction (SCLC) model, the conduction mechanism of the nitride films is closely related to electron trapping and detrapping in nitride-related electron traps [4]. For both devices, in the low voltage region (0 to 0.4 V) of the HRS, the thermally generated carrier migration inherent in the nitride film causes a low current, and the fitted curve shows an Ohmic conduction dependence (I∼V). As the voltages of the TiN/ZrN/TiN and TiN/HfN/ZrN/TiN devices rise to (0.4 to 1.3 V) and (0.4 to 0.9 V), respectively, the number of injected carriers exceeds the number of thermally generated carriers and trapping and detrapping of the inherent defects in the nitride, which leads to the conduction following the SCLC behavior of trap filling ($I \sim V^2$). At high voltages (>1.3 V for TiN/ZrN/TiN and >0.9 V for TiN/HfN/ZrN/TiN), all traps are filled with charge carriers, a conductive path is formed, and the current suddenly increases; the devices are SET from the HRS to the LRS. In the entire LRS region of both devices, the I-V curves are linear with a slope of 1, which is consistent with the Ohmic conduction mechanism. In standard SCLC theory, the current density J emitted by trap-controlled SCLC can be expressed as:

$$J = (\theta/\theta + 1)(9/8)\varepsilon_r\varepsilon_0\mu(V^2/L^3) \quad (1)$$

where $\theta = (N_C/N_t)\ \exp(E_cE_t)/kT$ is the ratio of the free electrons to the trapped electrons, N_C is the effective density of states in the conduction band, N_t is the number of empty electron traps, ε_0 is the dielectric constant of free space, ε_r is the relative permittivity, μ is the electron mobility, V is the applied voltage, and L is the film thickness.

We also present a schematic model of a TiN/ZrN/TiN device based on the formation and rupture of CFs, which is shown in Figs. 2 (b and c). The CF consists of nitrogen (N) vacancies in the device that are created mostly at the grain boundaries of the RS layer during the forming or SET process. The creation of N vacancies in ZrN devices is very similar to the creation of oxygen vacancies in metal oxide RRAM devices [4]. After forming or the SET process, the free N ions released from ZrN remain at the TiN/ZrN interface rather than being absorbed by TiN because the Gibbs free energy of TiN (−217 kJ/mol) is higher than that of ZrN (−336 kJ/mol), and nitrogen ions need more energy to be absorbed in TiN [18]. During the RESET process, the nitrogen ions drift back to the ZrN and recombine with the nitrogen vacancies, causing the filament to rupture. Due to the high thermal conductivity (50 W/mK) of ZrN, the local heating effect is not as severe as that in the metal oxide device, and the shape and size of the filament can be better controlled [8].

To control the switching voltage variation and switching stability of the TiN/ZrN/TiN device, we used a 3 nm HfN thin layer between the TE and 7 nm ZrN layer. The improved characteristics of the TiN/HfN/ZrN/TiN device are shown in Fig. 3. The device has SET and RESET voltages of approximately 0.8 and −0.6 V, respectively (Fig. 3a). The TiN/HfN/ZrN/TiN device has a smaller SET/RESET voltage change than the TiN/ZrN/TiN device (Fig. 3b). For TiN/HfN/ZrN/TiN devices with a speed of 45 ns, an AC endurance of up to 10^7 cycles is achieved (Fig. 3c) using a pulse height of 1.6 V for the SET operation and −1.5 V for the RESET operation. The retention of the TiN/HfN/ZrN/TiN device is measured at 100° C, and both the LRS and HRS exhibit high stability (Fig. 3d).

Authorized licensed use limited to: Nanyang Technological University. Downloaded on May 09,2020 at 07:26:29 UTC from IEEE Xplore. Restrictions apply.

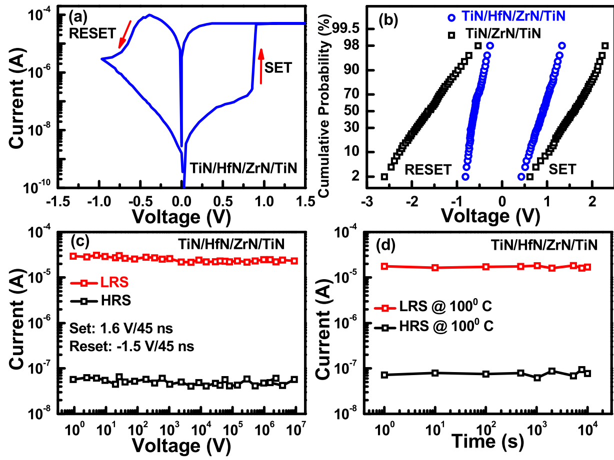

Fig. 3. (a) I-V curve for the TiN/HfN/ZrN/TiN device, (b) voltage distribution for the TiN/ZrN/TiN and TiN/HfN/ZrN/TiN devices, (c) AC endurance for the TiN/HfN/ZrN/TiN device and (d) retention at 100°C for the TiN/HfN/ZrN/TiN device.

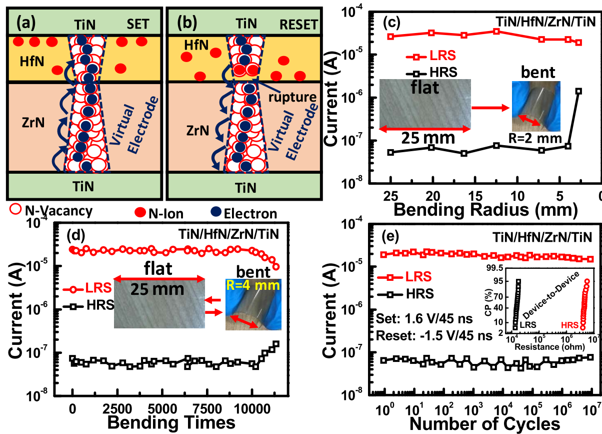

Fig. 4. (a and b) The CF model for the TiN/HfN/ZrN/TiN device. (c) Memory window of the TiN/HfN/ZrN/TiN device for different bending radii. (d) DC endurance characteristics of the TiN/HfN/ZrN/TiN device during bending from the flat condition to a radius of 4 mm for 10^4 times. (e) AC endurance test of the TiN/HfN/ZrN/TiN at a bending radius = 4 mm.

Fig. 4 (a) and (b) illustrate the CF model for the TiN/HfN/ZrN/TiN device. When a positive bias is applied to the TiN TE, N vacancies are generated in the ZrN layer and migrate to the TiN BE to form conical filaments in the ZrN layer. As the N vacancies in the ZrN layer increase, ZrN becomes electrically conductive and behaves like a "virtual electrode" [19]. It should be noted that the conductive virtual electrode, which is part of the CF, also consists of N vacancies. Now, the "virtual electrode" in the ZrN layer tends to be the seed for CF regrowth in the HfN layer. Based on the RS mechanism, the high uniformity is due to the limitation of the rupture point and recovery locations in the matrix layer near the HfN/ZrN interface. After the device switches to the HRS, the root of the CF does not dissolve completely during the RESET process. In the TiN/HfN/ZrN/TiN device, the CF is preferably connected or ruptures at the HfN/ZrN interface, and the ZrN layer behaves as a virtual electrode [19]. This RS mechanism enhances the uniformity and reduces the SET/RESET voltage variations of the TiN/HfN/ZrN/TiN device.

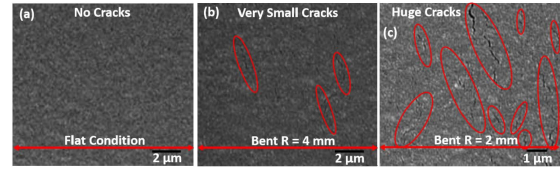

Fig. 5. (a) SEM image of the device in the flat condition, (b) when the device is bent to R = 4 mm and (c) when the device is bent R = 2 mm.

The flexible properties of the TiN/HfN/ZrN/TaN device are also investigated. During the measurements, the device is bent up to surface curvature radius of 25–2 mm. Figure 4(c) shows the values for various bending radii. The device exhibits a stable resistance ratio between the LRS and HRS without any degradation to mechanical bending from 25 to 4 mm but rapid degradation occurs for 2 mm bending. This degradation in the resistances is due to the increase in the sheet resistance of the RS layer and BE during the bending condition [20].

Fig. 4 (d) shows the endurance characteristics of the device after bending from a flat state to a 4 mm radius 12,000 times. Both the LRS and HRS are highly stable up to 10,000 bending cycles, after which the device shows degradation in both states. The first read operation is performed after the first bending cycle, and then a read operation is performed after every 200 bending cycles to measure the stability of the device. The AC endurance test is also investigated for a 4 mm bending radius at a read voltage of 0.3 V, and the result is shown in Fig. 4 (e). By using a pulse height of 1.6 V for the SET process and −1.5 V for the RESET process with a pulse width of 45 ns, the flexible device can maintain both LRS and HRS for up to 10^7 cycles without any degradation. The inset of Fig. 4(e) exhibits the consistency of LRS and HRS values among the measured results for the 20 devices. The high stability of the LRS and HRS confirms the high reproducibility of the device.

For experimental evidence, we obtain SEM images of the device in the flat and bent conditions, as shown Fig. 5. In Fig. 5 (a), there are no cracks visible for the device in the flat condition. For the device with a bending R = 4 mm, the crack density is much less, as observed from Fig. 5 (b), and the increase in the resistance of the ZrN layer due to the few cracks results in the maintenance of a good memory performance [13], [21]. In Fig. 5 (c), it is clear that there are many cracks in the device when R = 2 mm. These cracks lead to an increase in the ZrN layer resistance on the ITO/PET substrate, resulting in degradation of the device performance. Therefore, the device shows rapid degradation in the LRS and HRS when the device is bent to R = 2 mm.

IV. Conclusion

We investigated RRAM devices based on a ZrN RS layer. The device has excellent switching characteristics, such as a high AC durability and stable retention at high temperatures. In addition, the device fabricated with a HfN interfacial layer between the TE and ZrN exhibits small operational voltage variations and stable switching characteristics. The flexible device shows excellent switching characteristics when bent up to a radius of 4 mm. Finally, this report clearly establishes that the ZrN-based RRAM device studied herein has potential for flexible memory applications.

Authorized licensed use limited to: Nanyang Technological University. Downloaded on May 09,2020 at 07:26:29 UTC from IEEE Xplore. Restrictions apply.

References

[1] D. Kumar, R. Aluguri, U. Chand, and T.-Y. Tseng, "Conductive bridge random access memory characteristics of SiCN based transparent device due to indium diffusion," *Nanotechnology*, vol. 29, no. 12, Mar. 2018, Art. no. 125202, doi: 10.1088/1361-6528/aaa939.

[2] D. Kumar, R. Aluguri, U. Chand, and T.-Y. Tseng, "Enhancement of resistive switching properties in nitride based CBRAM device by inserting an Al_2O_3 thin layer," *Appl. Phys. Lett.*, vol. 110, no. 20, May 2017, Art. no. 203102, doi: 10.1063/1.4983465.

[3] D. Kumar, R. Aluguri, U. Chand, and T.-Y. Tseng, "One bipolar selector-one resistor for flexible crossbar memory applications," *IEEE Trans. Electron Devices*, vol. 66, no. 3, pp. 1296–1301, Mar. 2019, doi: 10.1109/TED.2019.2895416.

[4] Z. Zhang, B. Gao, Z. Fang, X. Wang, Y. Tang, J. Sohn, H.-S.-P. Wong, S. S. Wong, and G.-Q. Lo, "All-metal-nitride RRAM devices," *IEEE Electron Device Lett.*, vol. 36, no. 1, pp. 29–31, Jan. 2015, doi: 10.1109/LED.2014.2367542.

[5] M. L. Addonizio, A. Castaldo, A. Antonaia, E. Gambale, and L. Iemmo, "Influence of process parameters on properties of reactively sputtered tungsten nitride thin films," *J. Vac. Sci. Technol. A, Vac., Surf., Films*, vol. 30, no. 3, May 2012, Art. no. 031506, doi: 10.1116/1.3698399.

[6] A. B. Mei, O. Hellman, N. Wireklint, C. M. Schlepütz, D. G. Sangiovanni, B. Alling, A. Rockett, L. Hultman, I. Petrov, and J. E. Greene, "Dynamic and structural stability of cubic vanadium nitride," *Phys. Rev. B, Condens. Matter*, vol. 91, no. 5, Feb. 2015, Art. no. 054101, doi: 10.1103/PhysRevB.91.054101.

[7] R. Arvinte, J. Borges, R. E. Sousa, D. Munteanu, N. P. Barradas, E. Alves, F. Vaz, and L. Marques, "Preparation and characterization of CrNxOy thin films: The effect of composition and structural features on the electrical behavior," *Appl. Surf. Sci.*, vol. 257, no. 21, pp. 9120–9124, Aug. 2011, doi: 10.1016/j.apsusc.2011.05.109.

[8] Q. Zheng, A. B. Mei, M. Tuteja, D. G. Sangiovanni, L. Hultman, I. Petrov, J. E. Greene, and D. G. Cahill, "Phonon and electron contributions to the thermal conductivity of VNx epitaxial layers," *Phys. Rev. Mater.*, vol. 1, no. 6, Nov. 2017, Art. no. 065002, doi: 10.1103/PhysRevMaterials.1.065002.

[9] M. Kim and K. C. Choi, "Transparent and flexible resistive random access memory based on Al2O3Film with multilayer electrodes," *IEEE Trans. Electron Devices*, vol. 64, no. 8, pp. 3508–3510, Aug. 2017, doi: 10.1109/TED.2017.2716831.

[10] K. Qian, R. Y. Tay, M.-F. Lin, J. Chen, H. Li, J. Lin, J. Wang, G. Cai, V. C. Nguyen, E. H. T. Teo, T. Chen, and P. S. Lee, "Direct observation of indium conductive filaments in transparent, flexible, and transferable resistive switching memory," *ACS Nano*, vol. 11, no. 2, pp. 1712–1718, Feb. 2017, doi: 10.1021/acsnano.6b07577.

[11] S. Mondal, C. H. Chueh, and T. M. Pan, "High-performance flexible Ni/Sm_2O_3/ITO ReRAM device for low-power nonvolatile memory applications," *IEEE Electron Device Lett.*, vol. 34, no. 9, pp. 1145–1147, Sep. 2013, doi: 10.1109/LED.2013.2272455.

[12] Y. Ji, Y. Yang, S.-K. Lee, G. Ruan, T.-W. Kim, H. Fei, S.-H. Lee, D.-Y. Kim, J. Yoon, and J. M. Tour, "Flexible nanoporous WO_{3-x} nonvolatile memory device," *ACS Nano*, vol. 10, no. 8, pp. 7598–7603, Aug. 2016, doi: 10.1021/acsnano.6b02711.

[13] K. N. Pham, V. D. Hoang, C. V. Tran, and B. T. Phan, "TiO_2 thin film based transparent flexible resistive switching random access memory," *Adv. Natural Sci., Nanosci. Nanotechnol.*, vol. 7, no. 1, Mar. 2016, Art. no. 015017, doi: 10.1088/2043-6262/7/1/015017.

[14] Y. Chen, L. Li, X. Yin, A. Yerramilli, Y. Shen, Y. Song, W. Bian, N. Li, Z. Zhao, W. Qu, N. D. Theodore, and T. L. Alford, "Resistive switching characteristics of flexible TiO_2 thin film fabricated by deep ultraviolet photochemical solution method," *IEEE Electron Device Lett.*, vol. 38, no. 11, pp. 1528–1531, Nov. 2017, doi: 10.1109/LED.2017.2756444.

[15] K.-J. Lee, Y.-C. Chang, C.-J. Lee, L.-W. Wang, and Y.-H. Wang, "Bipolar resistive switching characteristics in flexible Pt/MZT/Al memory and Ni/NbO_2/Ni selector structure," *IEEE J. Electron Devices Soc.*, vol. 6, pp. 518–524, Feb. 2018, doi: 10.1109/JEDS.2018.2801278.

[16] X. Cao, Y. Han, J. Zhou, W. Zuo, X. Gao, L. Han, X. Pang, L. Zhang, Y. Liu, and S. Cao, "Enhanced switching ratio and long-term stability of flexible RRAM by anchoring polyvinylammonium on perovskite grains," *ACS Appl. Mater. Interfaces*, vol. 11, no. 39, pp. 35914–35923, Oct. 2019, doi: 10.1021/acsami.9b12931.

[17] Y. Cai, J. Tan, L. YeFan, M. Lin, and R. Huang, "A flexible organic resistance memory device for wearable biomedical applications," *Nanotechnology*, vol. 27, no. 27, Jul. 2016, Art. no. 275206, doi: 10.1088/0957-4484/27/27/275206.

[18] W. M. Haynes, *CRC Handbook of Chemistry and Physics*. Boca Raton, FL, USA: CRC Press, 2014.

[19] R. Zhang, H. Huang, Q. Xia, C. Ye, X. Wei, J. Wang, L. Zhang, and L. Q. Zhu, "Role of oxygen vacancies at the TiO_2/HfO_2 interface in flexible oxide-based resistive switching memory," *Adv. Electron. Mater.*, vol. 5, Apr. 2019, Art. no. 1800833, doi: 10.1002/aelm.201800833.

[20] R. Aluguri, R. Sailesh, D. Kumar, and T.-Y. Tseng, "Characteristics of flexible and transparent Eu_2O_3 resistive switching memory at high bending condition," *Nanotechnology*, vol. 30, no. 4, Jan. 2019, Art. no. 045202, doi: 10.1088/1361-6528/aae670.

[21] J. Shang, W. Xue, Z. Ji, G. Liu, X. Niu, X. Yi, L. Pan, Q. Zhan, X.-H. Xu, and R.-W. Li, "Highly flexible resistive switching memory based on amorphous-nanocrystalline hafnium oxide films," *Nanoscale*, vol. 9, no. 21, pp. 7037–7046, 2017, doi: 10.1039/C6NR08687J.

Authorized licensed use limited to: Nanyang Technological University. Downloaded on May 09,2020 at 07:26:29 UTC from IEEE Xplore. Restrictions apply.